Proceedings of the
7th Graz Brain-Computer Interface Conference 2017 DOI: 10.3217/978-3-85125-533-1-44

A COMPARISON OF OCULAR ARTIFACT REMOVAL METHODS FOR BLOCK DESIGN BASED ELECTROENCEPHALOGRAPHY EXPERIMENTS

R. J. Kobler[1], A. I. Sburlea[1], G. R. Müller-Putz[1]

[1]Institute of Neural Engineering, Graz University of Technology, Graz, Austria

E-mail: gernot.mueller@tugraz.at

ABSTRACT: Eye movements and their contribution to electroencephalographic (EEG) recordings as ocular artifacts (OAs) are well studied. Yet their existence is typically regarded as impeding analysis. A widely accepted bypass is artifact avoidance. OA processing is often reduced to rejecting contaminated data. To overcome loss of data and restriction of behavior, research groups have proposed various correction methods. State of the art approaches are data driven and typically require OAs to be uncorrelated with brain activity. This does not necessarily hold for visuomotor tasks. To prevent correlated signals, we examined a two block approach. In a first block, subjects performed saccades and blinks, according to a visually guided paradigm. We then fitted 5 artifact removal algorithms to this data. To test their stationarity regarding artifact attenuation and preservation of brain activity, we recorded a second block one hour later. We found that saccades and blinks could still be attenuated to chance level, while brain activity during rest trials could be retained.

INTRODUCTION

In the last two decades extensive research on the neural encoding of upper limb movement kinematics has been carried out [1]. Experiments on kinematics decoding typically comprise visuomotor (VM) tasks [2–4]. Such tasks inherently involve visual feedback e.g. the distance between a target and an end-effector. Naturally, subjects would foveate between or track objects of interest [5]. This is typically avoided in laboratory conditions by instructing subjects to fixate their gaze to an arbitrary fixation point and reduce blinking to a minimum [2, 3, 6].

We want to emphasize that solely removing frontal channels from the analysis, while allowing eye movements is not sufficient to attenuate ocular artifacts (OAs) [4]. Central and parietal channels would nonetheless exhibit high correlations with saccade directions [7].

If the protocol allows saccades and blinks, literature typically separates between three independent types of artifacts [7, 8]. (1) Corneo-retinal dipole (CRD) artifacts cause signal changes that depend on eyeball rotation size and direction [7]. (2) Eyelid artifacts emerge from blinks, eyelid saccades and post-saccadic eyelid movements [7]. They elicit a large potential and are generated by the eyelid, whose displacement changes the impedance between positively charged cornea and extraocular skin [8]. (3) The saccadic spike potential (SP) is most prominent on periorbital electrodes and believed to result from contraction of extra-ocular muscles [8].

In future, we plan to apply the methods developed here on decoding kinematics from continuous visuomotor tasks. Previous studies consistently reported significant decoding information in low frequency components ($<$2 Hz) [2, 3, 6, 9]. We therefore focus on CRD and eyelid movements, since SP artifacts emerge in a frequency range $>$20Hz [8].

An alternative strategy to OA avoidance is correction. Literature provides numerous offline correction methods. For a recent review see [10]. Most common methods are either source estimation [7, 11, 12] or regression based [13] or a hybrid variant [14]. They all assume a linear mixing model:

$$\mathbf{x}(t) = \mathbf{A}\mathbf{s}(t) = \mathbf{A}^{(b)}\mathbf{s}^{(b)}(t) + \mathbf{A}^{(a)}\mathbf{s}^{(a)}(t) \qquad (1)$$

with the scalp recordings $\mathbf{x}(t)$ at time t being a mixture of sources $\mathbf{s}(t)$. The mixing matrix $\mathbf{A}$ is unknown. It can be separated into mixing coefficients $\mathbf{A}^{(b)}$ for brain sources $\mathbf{s}^{(b)}(t)$ and $\mathbf{A}^{(a)}$ for artifact sources $\mathbf{s}^{(a)}(t)$.

Cortical control of an end-effector requires online removal of OAs. One approach is to use adaptive algorithms to iteratively estimate $\mathbf{A}^{(b)}$ [14]. An advantage is that they can track changes of mixing coefficients due to i.e. a changing electrode scalp interface. However, they assume uncorrelated brain activity and artifacts [10]. This does not necessarily hold true for VM tasks. An alternative correction approach proposed in [13] is to use a block based experimental design. In the first block subjects perform voluntary eye artifacts. Thereupon a correction model is learned and applied online in the main block, during which subjects perform the actual task. Here time invariant mixing coefficients are assumed. Consequently, artifacts and brain activity can be correlated during the actual experiment. If the correlated brain activity contributes negligibly to the estimated eye artifact signals, only the artifact fraction is removed.

To our knowledge literature lacks a thorough comparison of how the previously listed correction approaches perform on the described block design. We selected five representatives and assessed their artifact correction performance on held out data. The algorithms are briefly outlined in the remainder of this section.

 DOI: 10.3217/978-3-85125-533-1-44

EYE-REG: A regression based algorithm originally proposed for block design [13]. It requires designated EOG channels to compute vertical and horizontal estimates of eye artifact source signal $\hat{\mathbf{s}}^{(a)}(t)$. The model, defined in equation 1, can be rewritten as

$$\mathbf{x}(t) = \mathbf{A}^{(a)}\mathbf{s}^{(a)}(t) + \mathbf{n}(t) \quad (2)$$

with the brain activity considered as noise $\mathbf{n}(t)$. The authors used the least squares solution to calculate an estimate $\hat{\mathbf{A}}^{(a)}$. The cleaned channels $\mathbf{x}_c(t)$ are then:

$$\mathbf{x}_c(t) = \mathbf{x}(t) - \hat{\mathbf{A}}^{(a)}\hat{\mathbf{s}}^{(a)}(t) \quad (3)$$

If the empiric estimates $\hat{\mathbf{A}}^{(a)}$ and $\hat{\mathbf{s}}^{(a)}$ are close to the unknowns, we can recover the brain activity by inserting equation 2 in 3:

$$\mathbf{x}_c(t) = \mathbf{A}^{(a)}\mathbf{s}^{(a)}(t) + \mathbf{n}(t) - \hat{\mathbf{A}}^{(a)}\hat{\mathbf{s}}^{(a)}(t) \approx \mathbf{n}(t) \quad (4)$$

MARA[1]*:* Multiple Artifact Rejection Algorithm (MARA) is an independent component analysis (ICA) based algorithm [12]. ICA is used to estimate an unmixing matrix $\mathbf{V}$ that transforms equation 1 into:

$$\hat{\mathbf{s}}(t) = \mathbf{V}\mathbf{x}(t) = \mathbf{V}\mathbf{A}\mathbf{s}(t) \approx \mathbf{s}(t) \quad (5)$$

and recovers independent components (ICs) $\hat{\mathbf{s}}(t)$. *MARA* then applies a plug-and-play classifier to identify artifactual ICs and rejects them [12].

EYE-EEG[1]*:* Here, artifactual ICs are rejected based on a variance ratio metric [7]. An IC's variance is computed during designated saccade and fixation periods[2]. If their ratio exceeds a threshold, the IC is rejected. In [7] an eye tracker was employed to detect saccades and fixations.

REGICA[1]*:* Regression-ICA is a hybrid method [14]. The authors showed that artifactual ICs carry more ocular and less brain activity than scalp channels. Hence, they proposed to apply regression to artifactual ICs only.

EYE-SUB[1]*:* Artifact subspace subtraction is another approach to correct equation 1 for eye artifacts. Instead of using fixed linear combinations of EOG channels, like for regression, an artifact unmixing matrix $\mathbf{V}^{(a)}$ is computed. It recovers an estimate of the eye artifact signals $\hat{\mathbf{s}}^{(a)}(t)$:

$$\hat{\mathbf{s}}^{(a)}(t) = \mathbf{V}^{(a)}\mathbf{x}(t) \quad (6)$$

In combination with an estimated artifact mixing matrix $\hat{\mathbf{A}}^{(a)}$ equation 3 transforms to:

$$\mathbf{x}_c(t) = \mathbf{x}(t) - \hat{\mathbf{A}}^{(a)}\hat{\mathbf{s}}^{(a)}(t) = (\mathbf{I} - \hat{\mathbf{A}}^{(a)}\mathbf{V}^{(a)})\mathbf{x}(t) \quad (7)$$

The columns of $\hat{\mathbf{A}}^{(a)}$ are computed by finding the subspace which is maximally different between two conditions e.g. up vs. down saccades [11].

[1]We used the publicly available eeg-lab extension. Available online: `https://sccn.ucsd.edu/wiki/EEGLAB_Extensions`

[2]Fixations are defined as periods during which no eye movements happen [7].

MATERIALS AND METHODS

Participants: Five persons, aged 23.6±3.9 years, participated in this study. Three of them were female. All subjects had corrected to normal vision. They had already participated at least once in an EEG experiment before. All signed an informed consent after they were instructed about purpose and procedure of the study. The experimental procedure conformed to the declaration of Helsinki and was approved by the local ethics committee.

Stimulus Presentation: Subjects were seated in a shielded room at 1.4m distance to a computer screen (NEC Multisync 27" IPS TFT, 60Hz refresh rate, FullHD resolution). Stimuli were restricted to a square of 0.32 m x 0.32 m around the center of the screen ($\sim$13° x 13° visual angle).

Data Acquisition: EEG and EOG were recorded with a 64 channel ActiCap system connected to a BrainAmp amplifier. It sampled the data at a rate of 1 kHz and applied a first order highpass filter with a cutoff frequency of 0.016 Hz. 58 electrodes were placed at frontal, central, parietal and occipital sites according to the extended 10-20 system. The remaining 6 electrodes were placed on the outer canthi, infra and superior orbital to the left and right eye respectively. Ground and reference were placed on AFz and the right mastoid, respectively.

Experimental Procedure: The paradigm is illustrated in Figure 1. It defines four conditions. REST: subjects were instructed to fixate a blue sphere for 10 s. HORZ/VERT: the sphere moved on a continuous horizontal/vertical trajectory. Subjects were directed to accurately follow it with their gaze. BLINK: The sphere's vertical diameter shrunk 8 times for 0.5 s instructing subjects to blink once each time.

We decided to implement a visually guided paradigm to have control over saccades and blinks. It simplifies splitting the data into corresponding epochs. An eye tracker, originally required by *EYE-EEG*, was not necessary either. Figure 5 (right) illustrates the accordance of the stimulus with subject behavior (EOG derivatives).

The recording time was divided into 3 blocks. The first and last followed the presented paradigm. Both consisted of 27 trials (9 REST, 6 HORZ, 6 VERT and 6 BLINK). The choice of 27 trials and their partition was motivated by the requirements of the algorithms. Recordings of the middle block, lasting roughly 60 minutes, followed a different paradigm and will be published elsewhere.

Preprocessing: The EEG data was first downsampled to 250 Hz. To attenuate 50 Hz line noise, a 2$^{\text{nd}}$ order Butterworth bandstop filter was applied. Slow drifts were removed by a zero-phase 4$^{\text{th}}$ order Butterworth highpass filter with 0.4 Hz cutoff frequency.

We visually inspected the data for bad channels and flagged 1 to 3 channels across subjects. They were spherically interpolated. We then extracted epochs of 7 s starting 1 s after cue presentation and rejected 1.7±1.2 trials per block by visual inspection.

Three of the five algorithms, that we compare, process

 DOI: 10.3217/978-3-85125-533-1-44

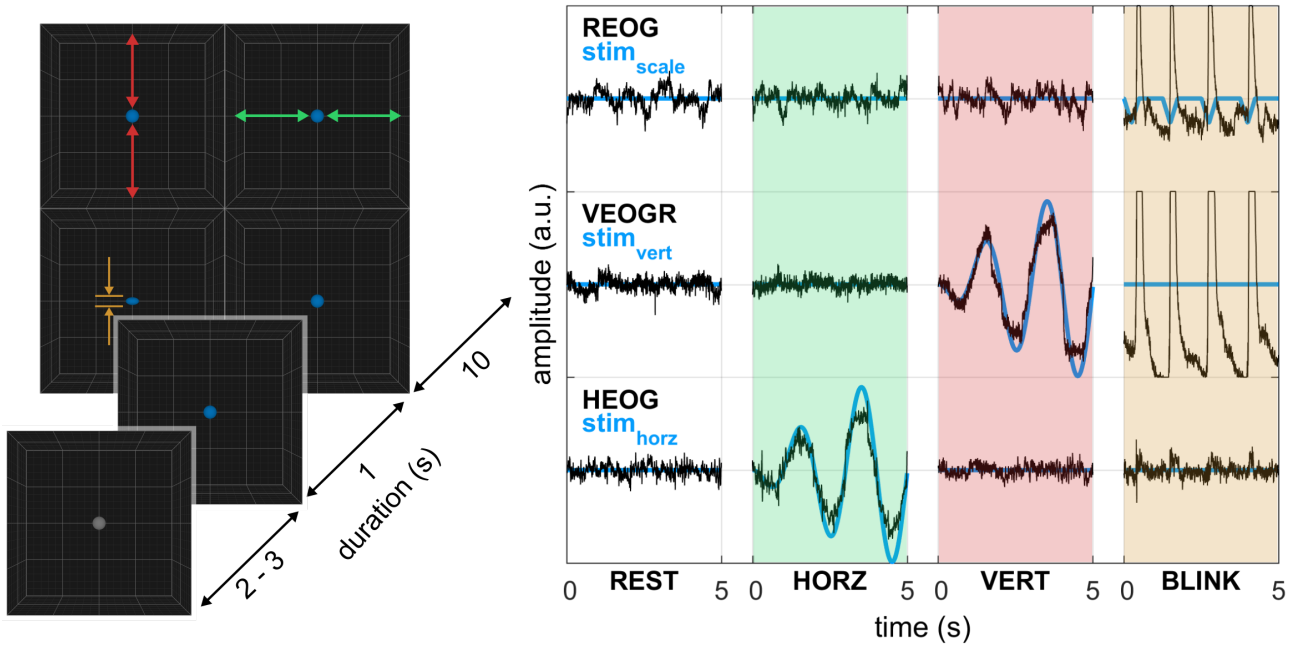

Figure 1: Experimental task. **(left)** The visual stimuli consisted of a 3D grid and a sphere, located in the center of the screen. Every trial started with a break lasting 2 to 3 seconds (uniformly distributed). Thereupon the sphere color changed to blue. After 1 s a condition dependent pattern was presented for 10 s. **(right)** First 5 s of the condition dependent patterns (blue). REST: the sphere remained in the center of the screen. HORZ: it moved along the horizontal plane according to a windowed sinusoid with a frequency of 0.5 Hz. VERT: the same movement but along the vertical plane. BLINK: the vertical diameter of the sphere changed, instructing the subject to blink. Additionally horizontal, vertical and radial EOG derivatives for selected trials of subject 1 are plotted (black).

the data in IC space. Before computing ICA we applied principal component analysis (PCA) on the 64 EEG/EOG channels and retained components explaining 99.9% of the variance. We then applied the extended Infomax algorithm to compute the unmixing matrix $\mathbf{V}$ of equation 5. The regression based algorithms require EOG components as artifact sources $\hat{\mathbf{s}}^{(a)}(t)$. The horizontal EOG (HEOG) derivative was computed as the difference between right and left outer canthi, vertical EOG left/right (VEOGL/R) as the difference between left/right superior and inferior electrode, and the radial EOG (REOG) component as the average of all six EOG electrodes.

Fixation, saccade and blink detection: EYE-EEG required separating the data into fixation and saccade periods. Since we asked subjects to avoid eye movements during REST condition, we used REST trials as fixation periods. For saccade detection the HEOG and VEOG[3] component were first lowpass filtered (zero-phase Butterworth, 2nd order, 20 Hz cutoff frequency). Horizontal/vertical saccade periods were extracted from HORZ/VERT condition trials if the absolute value of the H/VEOG component was above 10 µV for at least 200 ms. The sign was also used to split the data into left/right and up/down saccades.
Blink detection is also based on the lowpass filtered VEOG component. Samples during BLINK trials were set to be blink related if the VEOG amplitude was above 200 µV. The limits of these periods were expanded by 75 ms to include blink on- and offset.

[3]VEOG is the arithmetic mean of VEOGR and VEOGL.

EYE-REG: In [13] the authors argue to omit the REOG component, since it also captures considerable brain activity. We, therefore, used only HEOG and VEOGL/R as predictor variables for multiple linear regression.

EYE-SUB: First, penalized logistic regression (PLR) [11] with a regularization factor of 10^{-3} was applied to compute four artifact source signals $\hat{\mathbf{s}}^{(a)}(t)$ (4x1) that have a maximum magnitude difference between either left/right, up/down, blink/up or blink/down conditions. Similar to the regression approach, given $\hat{\mathbf{s}}^{(a)}(t)$, $\hat{\mathbf{A}}^{(a)}$ (64x4) can be computed by the pseudo inverse. The rest data was used to estimate a noise covariance matrix $\mathbf{R}_n$ (64x64). Considering $\mathbf{R}_n$, the unmixing matrix $\mathbf{V}^{(a)}$ (4x64) can be calculated by the regularized weighted least squares solution [11]:

$$\mathbf{V}^{(a)} = \left(\hat{\mathbf{A}}^{(a)T}\mathbf{R}_n\hat{\mathbf{A}}^{(a)} + \mathbf{\Lambda}\right)^{-1}\hat{\mathbf{A}}^{(a)T}\mathbf{R}_n \qquad (8)$$

with $\mathbf{\Lambda} = \lambda\mathbf{I}$ and regularization factor $\lambda = 10^{-4}$.

EYE-EEG: Similar to the original paper we set the threshold for the variance ratio to 1.1 [7].

REGICA: Precomputed ICs were flagged using the correlation between each IC and HEOG, VEOG with a threshold of 0.2. Multiple linear regression was applied to flagged ICs only. We used H/V/REOG as predictor variables.

Evaluation: All algorithms were fitted to the first block of data i.e. computation of ICA, regression weights and fitting of hyper parameters. The second block was solely employed for testing.

 DOI: 10.3217/978-3-85125-533-1-44

To assess artifact attenuation, we computed absolute values of Pearson correlation coefficients $|r|$ between EOG derivatives and each EEG channel. HEOG was used for HORZ, VEOG for VERT and blink periods during BLINK condition, respectively. Bootstrapping was applied to estimate chance level for $|r|$. Thus, we first merged the test trials of all subjects. We then randomly sampled 5 trials[4] of e.g. HORZ condition and computed $|r|$ with EEG channels of 5 random REST trials. The shuffling was repeated 5000 times for each condition. This yielded a 95%-quantile of 0.11 in every of the three conditions.

Preservation of neural activity was assessed twofold. Firstly, through computing the root mean squared error (RMSE) between cleaned $\mathbf{x}_c$ and uncleaned $\mathbf{x}$ signals during REST condition trials [14].

$$RMSE(k) = \sqrt{\frac{1}{N_s}\sum_{n}^{N_s}\left(x[k,n] - x_c[k,n]\right)^2} \qquad (9)$$

with k being the channel index and N_s the total number of samples in the test set.

Secondly, by computing the ratio between power spectral density of cleaned (Pxx_c) and uncleaned (Pxx) signals

$$Pxx_{ratio}(k,f) = \frac{Pxx_c(k,f)}{Pxx(k,f)} \qquad (10)$$

for each EEG channel k and frequency bin f [13]. We applied Welch's method to estimate the power spectral density for each trial and averaged across a subject's test trials.

RESULTS

Figure 2 depicts grand average topoplots of the 58 EEG channels after correction. The plots summarize mean test set performance for each metric and algorithm. The first row represents the uncorrected EEG. We observed typical eye artifact patterns for HORZ, VERT and BLINK conditions. Table 1 complements Figure 2. It lists mean and standard deviation across subjects for frontal, central and parietal channel groups.

Regarding the RMSE during REST, all algorithms exhibit a gradient from pre-frontal to occipital regions. *MARA* and *EYE-EEG* removed most activity, whereas *EYE-REG* and *EYE-SUB* achieve lowest RMSE across channel groups.

Figure 2 and Table 1 also summarize the absolute correlation $|r|$ between EEG channels and EOG derivatives after correction. One can clearly see that *MARA* could not identify ICs related to horizontal and vertical eye movements. This results in correlation values of up to 0.28 for frontal regions, which are clearly above the estimated chance level (0.11). The topoplots of the other algorithms show consistent attenuation of horizontal eye movements over scalp regions. Concerning vertical eye movements,

[4] Average number of trials in a subject's test set after rejection.

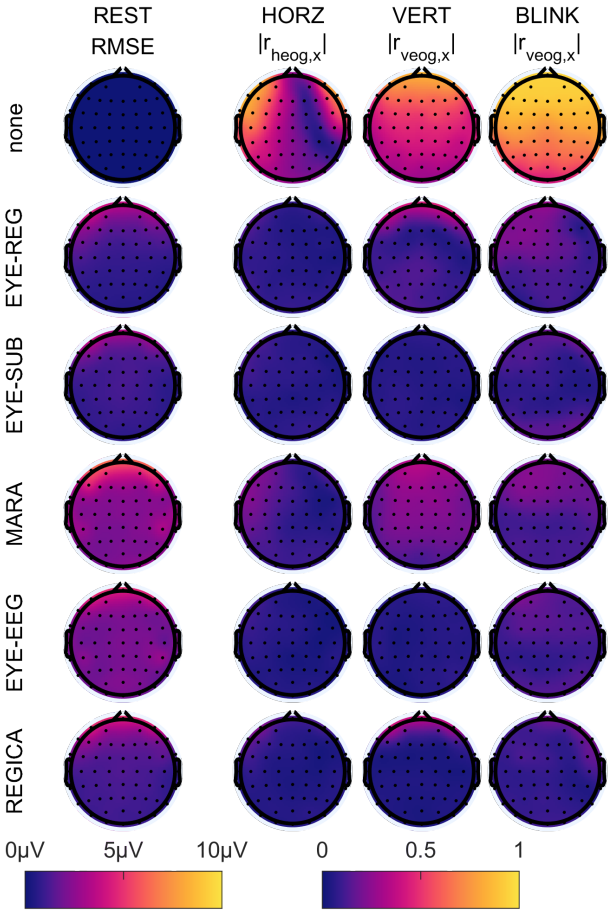

Figure 2: Topoplots (58 EEG channels) summarizing the average test set performance of the algorithms across subjects. (left) RMSE between corrected and uncorrected signal during REST condition, (right) absolute correlation $|r|$ with HEOG/VEOG/VEOG during HORZ/VERT/BLINK conditions.

EYE-SUB, *EYE-EEG* and *REGICA* could attenuate the correlation to similar levels as for horizontal ones. We also found that *EYE-SUB* and *REGICA* could attenuate blinks to chance level for frontal/central and parietal regions.

For visualization purposes, subsequent Figures show only the four algorithms that could attenuate artifact correlations to chance level, namely, *EYE-REG*, *EYE-SUB*, *EYE-EEG* and *REGICA*.

To estimate their performance decrease, we calculated group level means for train and test set. Figure 3 displays them for the average EEG channel. The barplots indicate mean and 95%-confidence interval for each condition and its associated metric. Non-overlapping train and test set confidence intervals, indicate a significant difference. The absolute correlation $|r|$ increased significantly for *EYE-SUB* (HORZ) and *EYE-EEG* (HORZ and BLINK).

The power spectral density ratio Pxx_{ratio} between corrected and uncorrected EEG revealed further differences across algorithms. Group level mean and its 95%-confidence interval are depicted in Figure 4 for frontal, central and parietal regions. *EYE-SUB* had its mean clos-

 DOI: 10.3217/978-3-85125-533-1-44

Table 1: Group level summary of performance metrics for frontal, central and parietal channel groups on the test set. Mean and standard deviation across subjects are stated per metric. The lowest value per metric and channel group is highlighted.

Condition	REST	HORZ	VERT	BLINK
Metric	RMSE	$\|r\|$	$\|r\|$	$\|r\|$
Unit	μV	-	-	-
Frontal (F3, Fz, F4)				
EYE-REG	1.8±0.5	0.06±0.04	0.11±0.07	0.19±0.15
EYE-SUB	**1.4±0.1**	0.08±0.03	**0.06±0.04**	0.11±0.08
MARA	3.1±1.0	0.12±0.13	0.28±0.25	0.23±0.08
EYE-EEG	2.3±0.4	**0.06±0.02**	0.06±0.05	0.15±0.09
REGICA	2.0±0.2	0.07±0.02	0.07±0.04	**0.10±0.04**
Central (C3, Cz, C4)				
EYE-REG	**1.0±0.4**	0.06±0.04	0.10±0.04	0.16±0.10
EYE-SUB	1.1±0.4	0.07±0.05	0.06±0.04	0.08±0.05
MARA	2.5±1.0	0.10±0.13	0.24±0.22	0.14±0.09
EYE-EEG	2.2±0.9	**0.05±0.02**	0.05±0.02	0.12±0.07
REGICA	1.3±0.3	0.05±0.03	**0.04±0.03**	**0.08±0.04**
Parietal (P3, Pz, P4)				
EYE-REG	**0.7±0.2**	0.07±0.04	0.12±0.06	0.12±0.06
EYE-SUB	1.0±0.4	0.06±0.04	0.07±0.04	0.10±0.08
MARA	2.2±1.0	0.10±0.13	0.20±0.21	0.12±0.03
EYE-EEG	2.1±0.8	**0.04±0.02**	0.06±0.04	0.10±0.08
REGICA	1.2±0.4	0.05±0.02	**0.04±0.03**	**0.09±0.03**

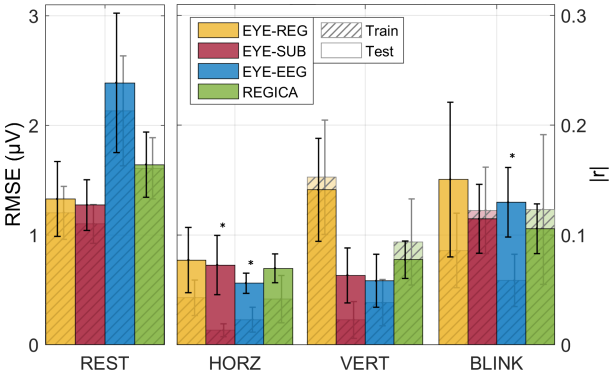

Figure 3: Algorithm performance on the average EEG channel for train (dashed) and test (solid) set. Mean and 95%-confidence interval across subjects are plotted for RMSE (left) and absolute correlation $|r|$ (right). Significant differences between train and test set are marked by *.

est to an ideal ratio of 1 and least variability of the mean across frequencies. *EYE-EEG* showed similar behavior for frontal, but larger attenuation in delta/theta frequency bands for central and parietal areas. *EYE-REG* resulted in largest mean attenuation in frontal areas, closely followed by *REGICA*. This improved considerably for central and posterior areas. We could also observe a larger variance of *REGICA* for the beta frequency band. It peaked in frontal channels.

DISCUSSION

In this work we compared five ocular artifact (OA) removal algorithms with regard to their applicability in a two step block design. We first trained the algorithms on a 5 min block of recordings. We then assessed their

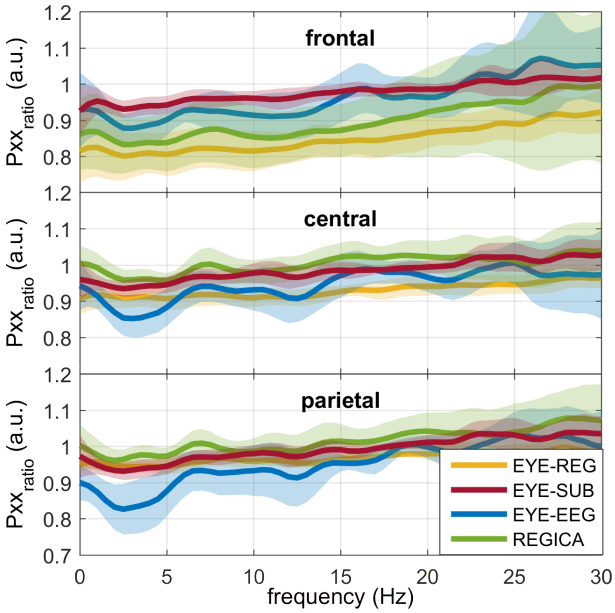

Figure 4: Mean and 95%-confidence interval of the group level power spectral density ratio Pxx_{ratio} for frontal (F3/z/4), central (C3/z/4) and parietal (P3/z/4) channels during REST condition. An ideal algorithm would yield a ratio of 1 for all frequencies.

OA removal quality on a test block recorded 60 minutes later. This approach implies a constant mixing matrix $\mathbf{A}^{(a)}$ for artifact sources. Our results, mainly Table 1 and Figure 3, give evidence that it is a reasonable assumption. We found that correlations for saccades and blinks could be attenuated to chance level, even 60 minutes after training. We emphasize that the difference between train and test set, displayed in Figure 3, captures not only the difference in time but also whether the data was used for parameter estimation. Therefore, we can not rule out if a significant difference was due to changing scalp projections or over-fitting on the train data.

As already pointed out in the introduction, allowing eye movements while only removing frontal channels is insufficient. Average correlations of up to 0.5 for uncorrected central and parietal channels (Figure 2) demonstrate the necessity for correction.

Regarding the algorithms, *MARA*, which did not rely on any label information, achieved lowest performance. While *EYE-SUB*, which required most information (annotated saccade and blink events), could attenuate artifacts to chance level and maintain low RMSE during REST condition. *REGICA* and *EYE-EEG* showed a tendency to achieve better attenuation for saccades and blinks in central and posterior areas but also to remove more brain activity.

The visually guided paradigm allowed us to control artifact occurrence. This simplified an automated annotation of artifact types (e.g. up/down saccades). In general, all algorithms tested here can be applied online. After artifact rejection and model calibration, which takes around 5 minutes, the correction process itself involves only matrix multiplications.

 DOI: 10.3217/978-3-85125-533-1-44

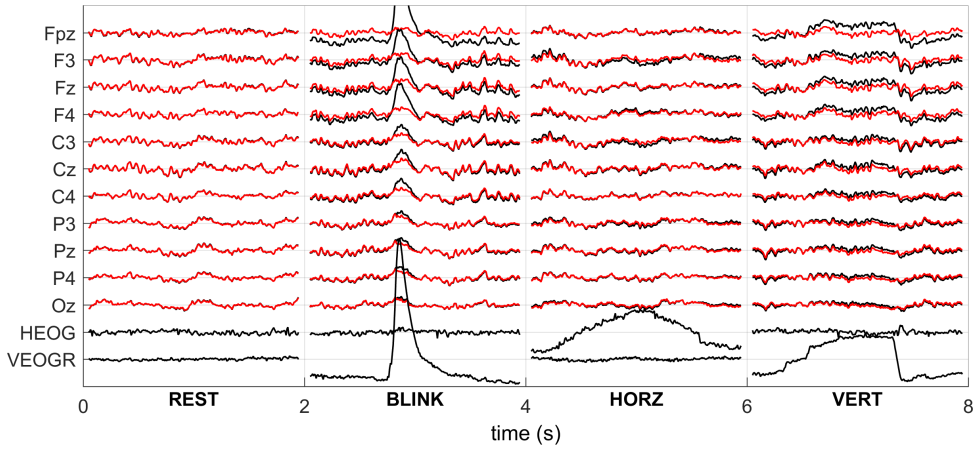

Figure 5: Representative examples in time domain for 2 s windows of selected trials. Displayed are 11 channels before (black) and after correction with *EYE-SUB* (red).

CONCLUSION

Based on the average performance on the test set, we found that *MARA* is not suitable for the investigated block design. Our results indicate, that artifact subspace subtraction (*EYE-SUB*) could achieve the best trade-off between attenuating eye artifacts and maintaining rest brain activity. Figure 5 depicts the difference between corrected and uncorrected EEG for representative trials and channels.

To complement our findings, we plan to analyze the effect on a kinematics decoder. This is a necessary step, since a significant performance drop was reported for a linear decoder after correction for OAs [6]. This demonstrates that eye artifacts were correlated with the dependent variables (x/y/z velocities). Our block design accounts for such a scenario, which encourages further research in this direction.

ACKNOWLEDGMENTS

This work was supported by the ERC Consolidator Grant 681231 ”Feel Your Reach”.

REFERENCES

[1] Müller-Putz GR, Schwarz A, Pereira J, *et al.* From classic motor imagery to complex movement intention decoding: The noninvasive Graz-BCI approach. In: Progress in Brain Research, 2016, vol. 228, 39–70.

[2] Bradberry TJ, Gentili RJ, Contreras-Vidal JL. Reconstructing Three-Dimensional Hand Movements from Noninvasive Electroencephalographic Signals. Journal of Neuroscience. 2010;30(9):3432–3437.

[3] Ofner P, Müller-Putz GR. Using a noninvasive decoding method to classify rhythmic movement imaginations of the arm in two planes. IEEE Transactions on Biomedical Engineering. 2015;62(3):972–981.

[4] Úbeda A, Azoín J, Chavarriaga R, *et al.* Evaluating decoding performance of upper limb imagined trajectories during center-out reaching tasks. In 2016 IEEE International Conference on Systems, Man, and Cybernetics. 2016, 252–257.

[5] Sailer U, Flanagan JR, Johansson RS. Eye–Hand Coordination during Learning of a Novel Visuomotor Task. Journal of Neuroscience. 2005;25(39):8833–8842.

[6] Kim JH, Bießmann F, Lee SW. Decoding three-dimensional trajectory of executed and imagined arm movements from electroencephalogram signals. IEEE Transactions on Neural Systems and Rehabilitation Engineering. 2015;23(5):867–876.

[7] Plöchl M, Ossandón JP, König P. Combining EEG and eye tracking: identification, characterization, and correction of eye movement artifacts in electroencephalographic data. Frontiers in Human Neuroscience. 2012;6(October):278.

[8] Keren AS, Yuval-Greenberg S, Deouell LY. Saccadic spike potentials in gamma-band EEG: Characterization, detection and suppression. NeuroImage. 2010;49(3):2248–2263.

[9] Waldert S, Preissl H, Demandt E, *et al.* Hand movement direction decoded from MEG and EEG. Journal of Neuroscience. 2008;28(4):1000–8.

[10] Urigüen JA, Garcia-Zapirain B. EEG artifact removal-state-of-the-art and guidelines. Journal of Neural Engineering. 2015;12(3):31001.

[11] Parra LC, Spence CD, Gerson AD, *et al.* Recipes for the linear analysis of EEG. NeuroImage. 2005;28(2):326–341.

[12] Winkler I, Brandl S, Horn F, *et al.* Robust artifactual independent component classification for BCI practitioners. Journal of Neural Engineering. 2014;11(3):035013.

[13] Schlögl A, Keinrath C, Zimmermann D, *et al.* A fully automated correction method of EOG artifacts in EEG recordings. Clinical neurophysiology. 2007;118(1):98–104.

[14] Klados MA, Papadelis C, Braun C, *et al.* REG-ICA: A hybrid methodology combining Blind Source Separation and regression techniques for the rejection of ocular artifacts. Biomedical Signal Processing and Control. 2011;6(3):291–300.